

# Stereotyped connectivity and computations in higher order olfactory neurons

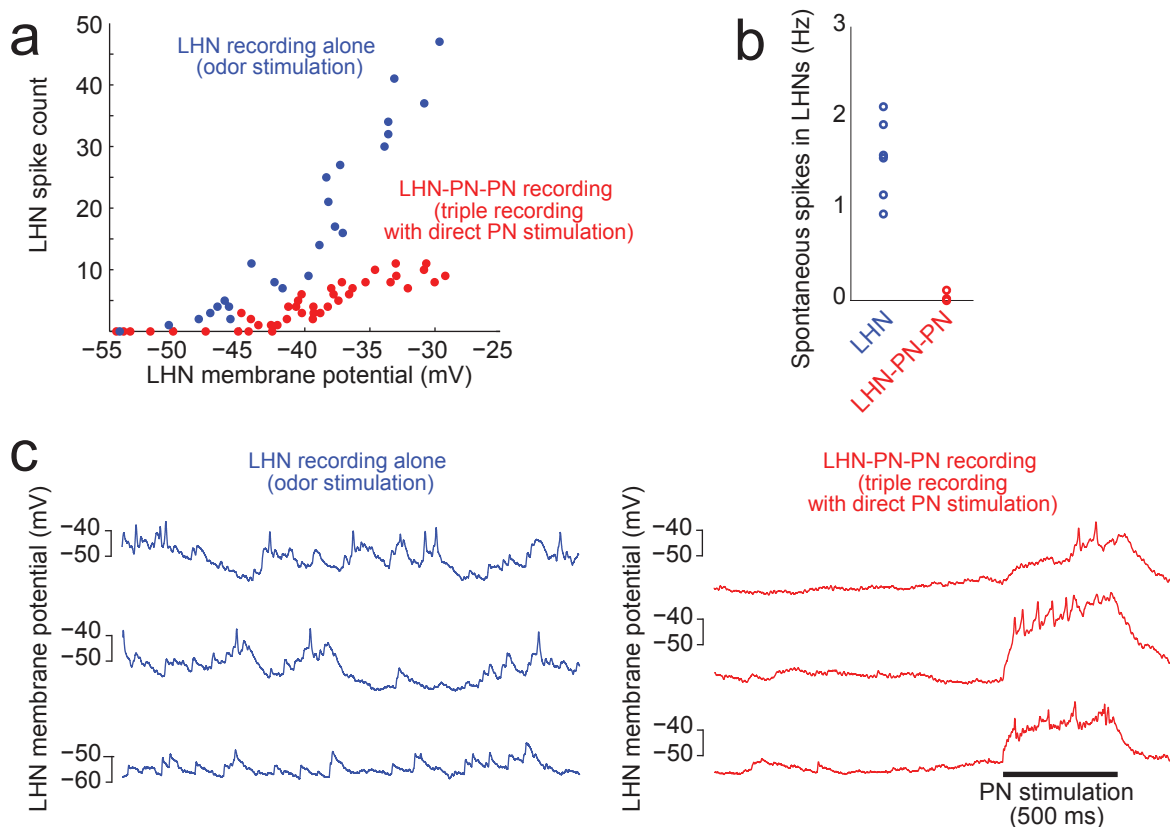
Mehmet Fisek and Rachel I. Wilson

## Supplementary Table 1: Genotypes

The genotypes used by figure are as follows:

Figure 1a	<i>UAS-C3PA-GFP;UAS-SPA-GFP/nsyb-Gal4</i>
Figure 1b	<i>pJFRC7-20XUAS-IVS-mCD8::GFP(attp40)/+;GMR73B12-Gal4/+</i>
Figure 1c	<i>pJFRC7-20XUAS-IVS-mCD8::GFP(attp40)/+; GMR44G08-Gal4/+</i>
Figure 1d	<i>Mz671-Gal4,UAS-CD8:GFP</i>
Figure 1e	<i>NP6099-Gal4,UAS-CD8:GFP</i>
Figure 2a	<i>pJFRC7-20XUAS-IVS-mCD8::GFP(attp40)/+;GMR48F03-Gal4/+</i> and <i>pJFRC7-20XUAS-IVS-mCD8::GFP(attp40)/+;GMR73B12-Gal4/+</i>
Figure 2b	<i>pJFRC7-20XUAS-IVS-mCD8::GFP(attp40)/+;GMR12H12-Gal4/+</i> and <i>pJFRC7-20XUAS-IVS-mCD8::GFP(attp40)/+; GMR44G08-Gal4/+</i>
Figure 2c,e	<i>Mz671-Gal4,UAS-CD8:GFP</i>
Figure 2d,f	<i>NP6099-Gal4,UAS-CD8:GFP</i>
Figure 3 LHN, DM1 PN pairs LHN, DM2 PN pairs  LHN, DM4 PN pairs LHN, DL5 PN pairs LHN, DM6 PN pairs LHN, DC1 PN pairs	<i>NP5221-Gal4,Mz671-Gal4;UAS-CD8:GFP</i> <i>Mz671-Gal4,UAS-CD8:GFP;c3l5-Gal4,UAS-CD8:GFP</i> and <i>GH146-Gal4,UAS-CD8GFP/Mz671-Gal4,UAS-CD8:GFP</i> and <i>NP5221-Gal4,UAS-CD8:GFP/Mz671-Gal4,UAS-CD8:GFP</i> <i>NP3062-Gal4,UAS-CD8:GFP;Mz671-Gal4,UAS-CD8:GFP</i> <i>NP3062-Gal4,UAS-CD8:GFP;Mz671-Gal4,UAS-CD8:GFP</i> <i>NP3062-Gal4,UAS-CD8:GFP;Mz671-Gal4,UAS-CD8:GFP</i> <i>Mz671-Gal4,UAS-CD8:GFP;c3l5-Gal4,UAS-CD8:GFP</i>
Figure 4 LHN, DM1 PN, DM2 PN triplets LHN, DM1 PN, DM4 PN triplets	<i>NP5221-Gal4,Mz671-Gal4;c3l5-Gal4,UAS-CD8:GFP</i> <i>NP3062-Gal4,UAS-CD8:GFP;NP5221-Gal4,Mz671-Gal4</i>
Figure 5 Lateral Horn Neurons DM1 PNs DM4 PNs	<i>Mz671-Gal4,UAS-CD8:GFP</i> <i>NP5221-Gal4,UAS-CD8:GFP</i> <i>NP3062-Gal4,UAS-CD8:GFP;</i>
Figure 6	<i>NP6099-Gal4;GH146-Gal4/UAS-C3PA-GFP;UAS-SPA-GFP/+</i>
Figure 7a,b LHNs DP1m PNs LHN DP1m pairs (blue points)	<i>NP6099-Gal4,UAS-CD8:GFP</i> <i>GH146-Gal4/UAS-C3PA-GFP;UAS-SPA-GFP/+</i> <i>NP6099-Gal4/+;GH146-Gal4/UAS-C3PA-GFP;UAS-SPA-GFP/+</i>
Figure 7c Wild type LHNs <i>Orco</i> <sup>2</sup> LHNs <i>IR64</i> <sup>MB05283</sup> LHNs	<i>NP6099-Gal4,UAS-CD8:GFP</i> <i>NP6099-Gal4,UAS-CD8:GFP;+/+;Orco</i> <sup>2</sup> <i>NP6099-Gal4,UAS-CD8:GFP;+/+;Ir64a</i> <sup>MB05283</sup>
Figure 8b, c LHNs in intact preparations LHNs w/ transection of iPN/ePN axons	<i>NP6099-Gal4,UAS-CD8:GFP</i> <i>NP6099-Gal4,UAS-CD8:GFP/+;GH146-Gal4,UAS-CD8:GFP/+</i>
Figure 8e,f,g Type I LHNs Type II LHNs Lateral horn local neurons	same as Figure 2a same as Figure 2b <i>pJFRC7-20XUAS-IVS-mCD8::GFP(attp40)/+;GMR23F06-Gal4/+</i>

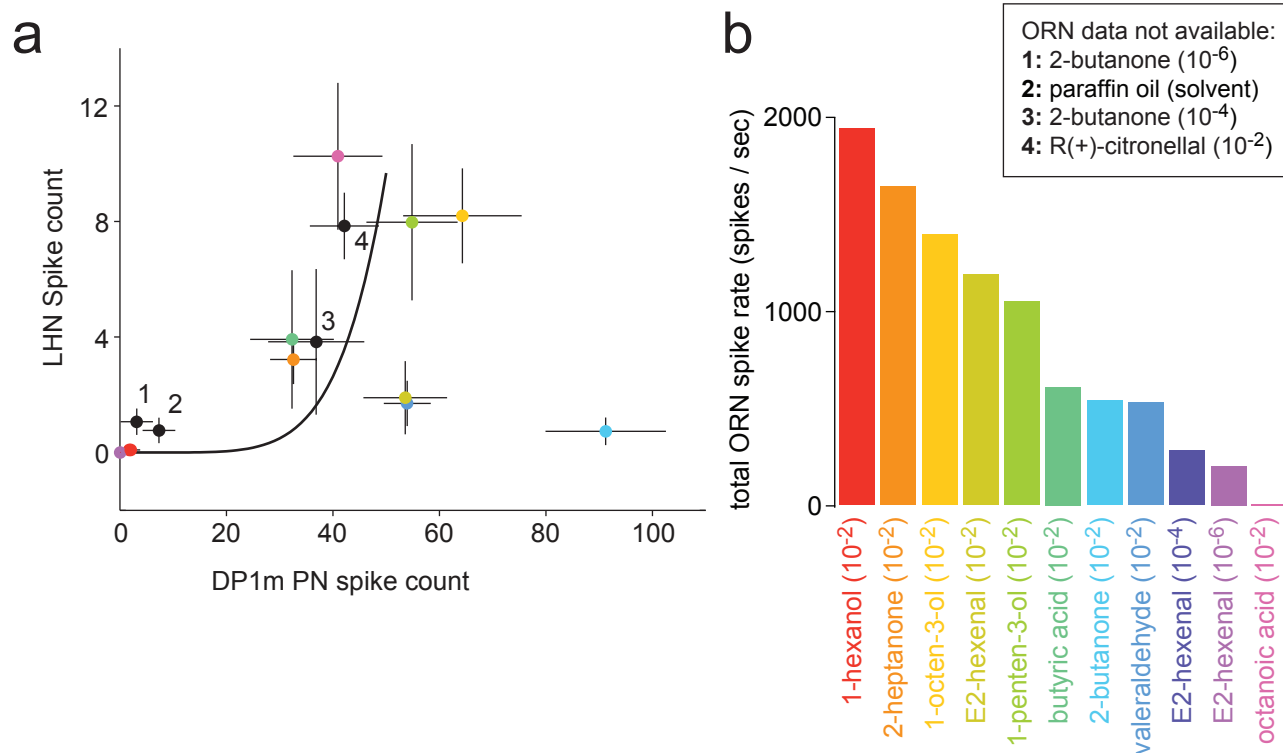
In addition to the glomeruli shown in Fig. 3 (and listed above in the corresponding section), we also targeted additional glomeruli for paired recordings from PNs and *Mz671* neurons, as noted in the text; these were the following glomeruli, with the Gal4 lines used to target them in parentheses: VA4 / VC1 / VC2 (*NP5221-Gal4*), VL2a (*NP3062-Gal4*), VM2 (*NP3481-Gal4* and *NP3062-Gal4*), VM7 (*GHI46-Gal4*). *NP6099-Gal4* was obtained from the Drosophila Genetic Resource Center (DGRC) at the Kyoto Institute of Technology. The following stocks were obtained from the Bloomington Stock Center: *Ir64a*<sup>MB05283</sup> (#24610), *nsyb-Gal4* (#39171), *GMR48F03-Gal4* (#50373, type I LHNs), *GMR73B12-Gal4* (#39814, type I LHNs), *GMR12H12-Gal4* (#48534, type II LHNs), *GMR44G08-Gal4* (#50216, type II LHNs), *GMR23F06-Gal4* (#49036, lateral horn local neurons). Genotypes were previously published as follows: *Mz671-Gal4*, *NP6099-Gal4*, and *NP5221-Gal4* (ref. 18); *nsyb-Gal4* (also known as *GMR57C10-Gal4*) and all other *GMR* lines (ref. 21); *UAS-C3PA-GFP* and *UAS-SPA-GFP* (these transgenes express different variants of PA-GFP under UAS control; ref. 14); *UAS-CD8:GFP* (ref. 40); *c315a-Gal4* (ref. 41); *GHI46-Gal4* (ref. 42); *NP3062-Gal4* (ref. 43); *NP3481-Gal4* (ref. 44); *Orco2* (ref. 24); *Ir64a*<sup>MB05283</sup> (ref. 26). *pJFRC7-20XUAS-IVS-mCD8::GFP(attP40)* is described in ref. 45 and was initially published in another insertion site (attP2)<sup>46</sup>. The *GMR* lines used here that have not been previously published are as follows: *GMR48F03-Gal4* (type I LHNs) labels ~10 neurons; *GMR73B12-Gal4* (type I LHNs) labels ~10 neurons; *GMR12H12-Gal4* (type II LHNs) labels ~20 neurons; *GMR44G08-Gal4* (type II LHNs) labels ~20 neurons; *GMR23F06-Gal4* (lateral horn local neurons) labels ~25 neurons. These numbers were obtained by visually inspecting confocal images publicly available at <http://flweb.janelia.org> (ref. 21).



### Supplementary Figure 1. Spontaneous activity modulates excitability in *Mz671* neurons.

The spike counts recorded in *Mz671* neurons in triple recording experiments were substantially lower than those obtained in recordings from the same neurons with olfactory stimulation (compare Figs. 4 and 5), even when the PNs were firing at similar rates. This discrepancy may be attributable to several causes. First, glomeruli other than DM4 may be recruited by low concentrations of the odor (methyl acetate), and these glomeruli might be presynaptic to these LHNs. If so, then the LHN would fire at a higher rate than we would expect based on the activity of DM4 alone. There is evidence that methyl acetate is specific for DM4 at these concentrations (Olsen et al., 2010), but this idea is still difficult to completely exclude. Second, there could be more than one DM4 PN. If so, we would be stimulating more PNs with odor versus with current injection. This is unlikely, because when we expressed PAGFP pan-neuronally and photoactivated the DM4 glomerulus, we found only one DM4 PN (data not shown). Third, LHNs may exhibit different excitability in the two types of experiments. In support of this idea, there was a systematic difference in the stimulus-evoked change in LHN spike rate for a given change in LHN membrane potential (**panel a**). Moreover, both spontaneous EPSPs and spikes were systematically reduced in the triple recordings versus (**panels b and c**; each point in **panel b** is a different experiment). In the triple recordings, we hyperpolarized the two PNs below their normal resting potential, thereby preventing them from spiking outside the stimulation window. In any given triple recording, we are thereby silencing two of the four known PN inputs to the LHN. This likely explains why spontaneous EPSPs are suppressed. In sum, we conclude that the LHN dendrites are likely somewhat hyperpolarized in the triple recordings, due in part to reduced spontaneous PN input, which diminishes the recruitment of voltage-dependent conductances in LHNs, thereby decreasing postsynaptic depolarization in response to PN spikes, and inhibiting postsynaptic spike generation.

Methods for analysis in **panel a**: LHN spikes were detected and then the LHN membrane potential was low-pass filtered to remove spikes. Trials were then sorted according to LHN spike count, binned into groups of 10, and averaged within each bin. Using these trial-averaged traces, we measured the membrane potential over a window of time. For the triple recordings, this was a 400-ms window starting 100 ms after the onset of current injection in the PN. In odor delivery experiments, there is a variable response delay, so we used a variable window. To find this window, we set a threshold (equal to 3 SDs above the baseline) for each trial-averaged trace, and we defined a 500 ms window starting at the first threshold crossing. Each point in **panel a** plots the average spike count and average membrane potential for a single bin.

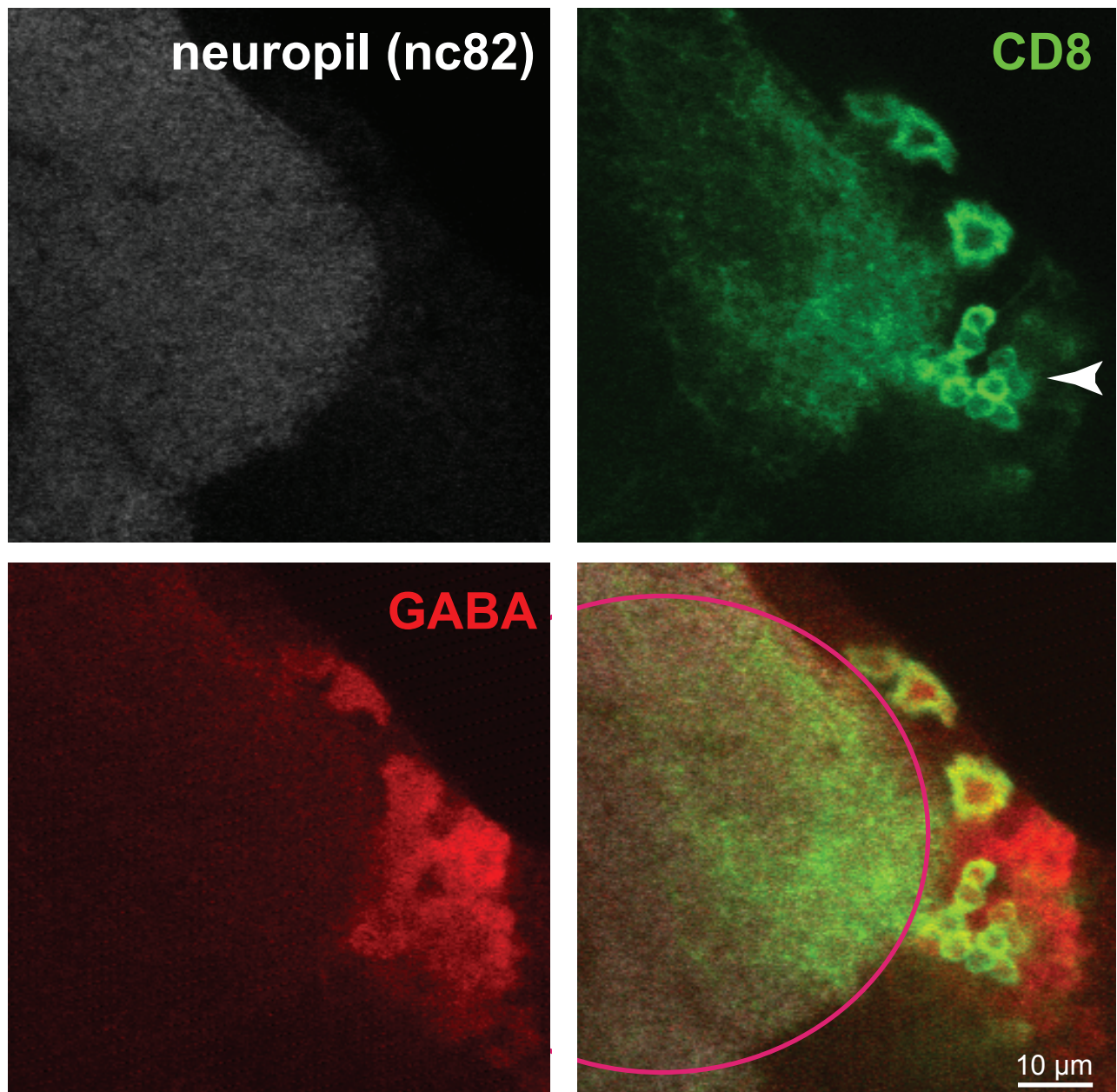


**Supplementary Figure 2. Inhibition in NP6099 neurons does not depend on total network activity.**

**a**, This panel contains the same data as in Fig. 7a (top, magenta symbols), but with stimuli color-coded. The smooth curve reproduces the fitted line from Fig. 7a (bottom).

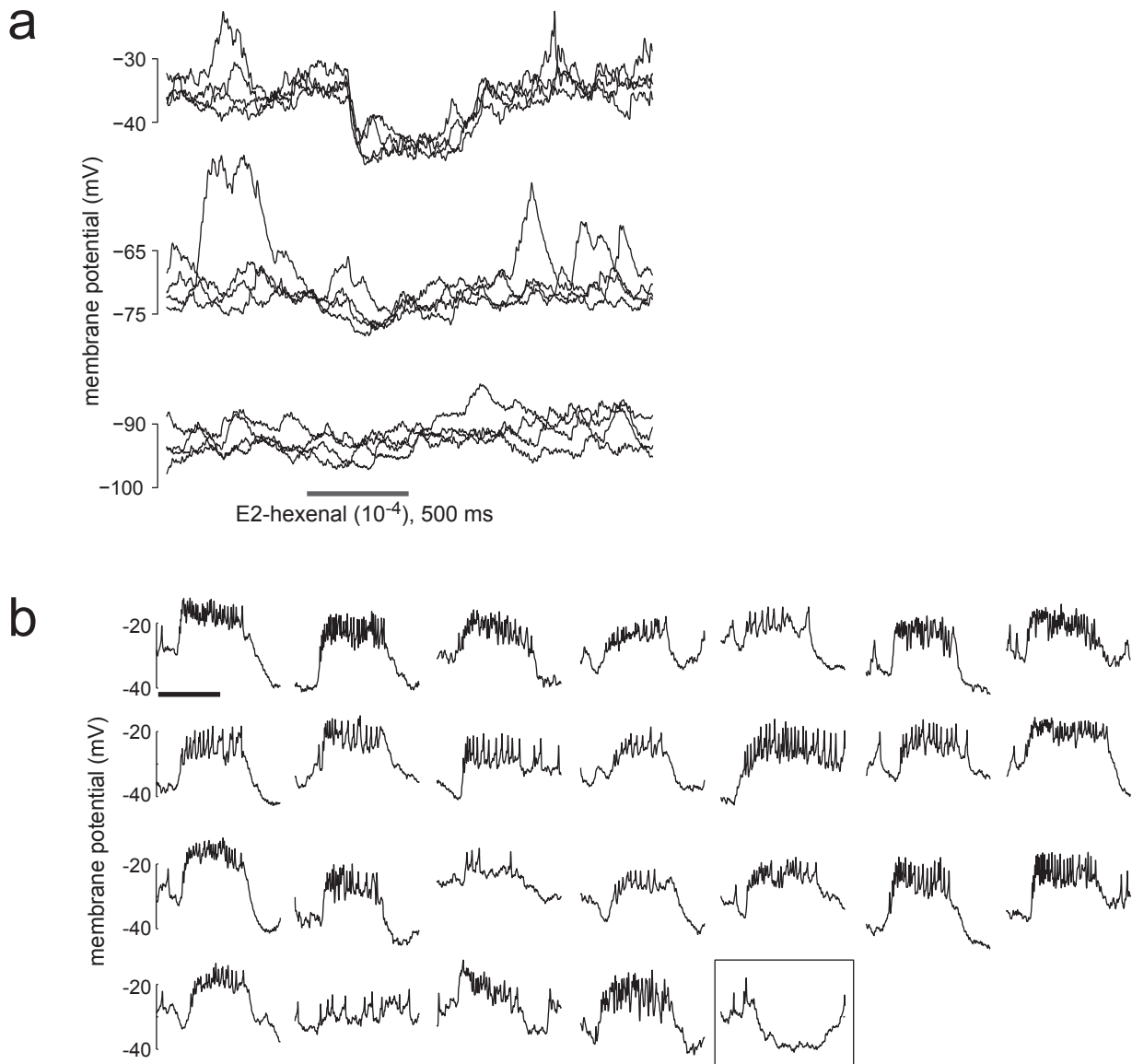
**b**, The total amount of olfactory receptor neuron activity for each stimulus, obtained by summing across the firing rates for all receptor types measured by Hallem et al. 2006. Color codes are the same as in panel a. (For the four numbered stimuli in black from panel a, olfactory receptor neuron data are not available.)

Note that the largest relative suppression in the LHN response (relative to the DP1m response) is observed for E2-hexenal ( $10^{-2}$ ), valeraldehyde ( $10^{-2}$ ), and 2-butanone ( $10^{-2}$ ). By comparison, relatively little suppression is observed for 1-penten-3-ol ( $10^{-2}$ ) and 1-octen-3-ol ( $10^{-2}$ ). There is no systematic relationship between the amount of suppression and the amount of total activity elicited in ORNs. Thus, the inhibition which suppresses these responses must be selective for the chemical composition of an odor (presumably therefore reflecting input from a small number of glomeruli), and is not simply driven by total network activity.



### Supplementary Figure 3. GABAergic local neurons in the lateral horn.

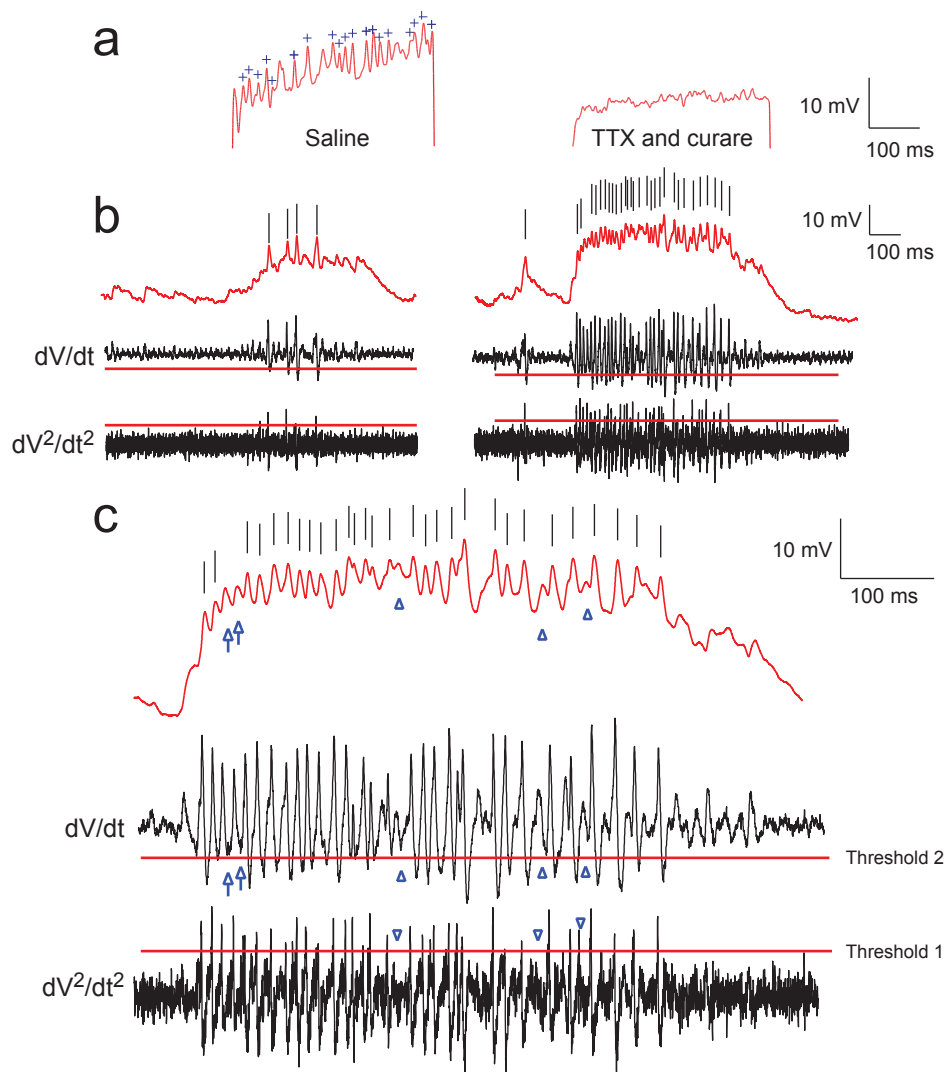
Single confocal sections through the lateral horn of a brain triple immunostained for neuropil (nc82), CD8, and GABA. Dorsal is up, lateral is right. Expression of CD8:GFP is driven by a Gal4 line with a restricted expression pattern (*GMR23F06-Gal4*). Single-cell dye fills from this Gal4 line demonstrate that these neurons are local to the lateral horn (Figure 8). Their somata lie in a cluster just lateral and slightly ventral to the lateral horn neuropil (arrowhead), and all these somata are GABA-positive, although not all GABA-positive somata in this cluster express CD8:GFP. In the overlay, a magenta circle indicates the approximate boundary of the lateral horn (as in Figures 1 and 8). Similar results were obtained in three brains.



**Supplementary Figure 4. Type II LHNs, but not type I LHNs, receive prominent odor-evoked inhibition.**

**a**, Responses of a typical *NP6099* neuron to a stimulus that elicits prominent hyperpolarization. In different trials, we manipulated the membrane potential of the LHN by injecting different amounts of current via the patch pipette. Note that odor-evoked hyperpolarization increases at more depolarized holding potentials, indicating that inhibition is at least partly postsynaptic.

**b**, In a single case, we observed odor-evoked hyperpolarization in a type I LHN. This was noted as part of our general survey of type I LHNs labeled by *GMR48F03-Gal4* and *GMR73B12-Gal4* (Figs. 1b and 2a). In addition to the core odor set shown in Fig. 2a, we used 26 additional odors in various recordings in the course of this survey, in order to determine if any of them elicited hyperpolarization. We held cells at a depolarized potential during these trials (-40 to -30 mV) to better reveal any inhibition that might be present. Shown here are responses to these 26 odors, only the last of which elicited any hyperpolarization. This example shows that type I cells can receive odor-evoked inhibition, but is still consistent with the conclusion this inhibition is much less prominent than in type II cells. (Odors are : 2,3-butanedione, 2-heptanone, 2-octanone, 3-octanol,  $\alpha$ -pinene, benzaldehyde, butyric acid, cis-3-hexen-1-ol, beta-citronellal, cyclohexanone, ethyl butyrate, ethyl caproate, ethyl cinnamate, ethyl lactate, ethyl propionate, fenchone,  $\gamma$ -octalactone, ginger oil, hexyl acetate, linalool, nerol, phenethyl acetate, pyrrolidine, triethylamine, valeraldehyde, isoamylamine; all dilutions are  $10^{-2}$ ; horizontal bar in first panel shows 500 ms odor stimulus period.)



### Supplementary Figure 5. Spike detection in LHNs.

Action potentials recorded from LHN somata tend to be unusually small. In order to verify that the fastest events we observe in the voltage trace are indeed action potentials, we confirmed that these small rapid events can be elicited with depolarizing current injection, and that they are sensitive to TTX (**panel a**). We also noted that the rate of these events grows with increasing depolarizing current injection, as expected.

In order to detect and count these events, we used a two-threshold algorithm. We identified the events that were both the fastest the rise and the fastest to decay, using an algorithm that thresholded the second and first derivatives of the voltage trace with positive and negative thresholds, respectively (see traces below **panels b and c**). Thresholds were determined on a cell-by-cell basis. Spikes that were automatically detected are marked with vertical bars. Automated detection was robust a low firing rates (**panel b**, left). However, at high firing rates, action potential height decreased. Therefore, thresholds were adjusted at high firing rates, and each trace was also individually inspected, and missed spikes were corrected (**panel c**). Arrows point to missed spikes that were missed by the algorithm and then subsequently corrected. For comparison, arrowheads point to fluctuations in the voltage that were not subsequently marked as spikes. These examples show that there was a clear separation between spikes and non-spikes based on the rates of change in the voltage traces. In order to ensure that the subjectivity of this process does not bias our results in Fig. 5b, we blinded the person performing the analysis to stimulus concentrations.